Marine and Petroleum Geology xxx (xxxx) xxx-xxx

Contents lists available at ScienceDirect

Marine and Petroleum Geology

journal homepage: http://ees.elsevier.com

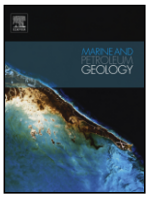

Research paper

Seismic velocity-depth relation in a siliciclastic turbiditic foreland basin: A case study from the Central Adriatic Sea

Paolo Mancinelli *, Vittorio Scisciani

Dipartimento di Ingegneria e Geologia, Università G. d'Annunzio di Chieti-Pescara, Via dei vestini 31, 66013, Chieti, Italy

ARTICLE INFO

Keywords
Adriatic foreland
Velocity-depth relation
Pliocene-Quaternary succession

ABSTRACT

Starting from reprocessed seismic profiles and borehole data, we investigate the Central Adriatic foredeep basin by deriving velocity depth trend of the Pliocene-Quaternary (PQ) siliciclastic succession (mainly composed by shales and sands). Relying on independent approaches to map two-way time (TWT) thickness of the PQ deposits, we converge on testing linear and exponential functions to predict V_P depth trend. Results suggest that for large (>1500 m) thicknesses of the PQ deposits best fit is achieved by the exponential function $V_P(z) = c\, z^{(1-n)}$ while for shallower and thinner deposits, a linear function like $V_P(z) = V_0 + k\, z$ provides the best fitting estimates. We also investigate anomalies in velocity trend with depth and suggest that velocity drops observed within the PQ succession at significant depth (2500–3500 m) may reflect overpressured deposits. This hypothesis is consistent with the Apennine compression and high sedimentation rates in Central Adriatic during the Pliocene-Quaternary. Finally, we stress the importance of considering vertical-component phenomena and their time evolution when modeling foreland basins.

1. Introduction

The Adriatic Sea is interposed between the Apenninic and Dinaric thrust and fold belts. It represents one of the most challenging study area over the entire Mediterranean region, due to its complex structural setting. Starting from the Cretaceous, the asynchronous development of the Alpine, Dinaric and Apenninic orogens affected this area, that was interpreted as the remnant of the Adria microplate (e.g. Vai, 2001; Stampfli et al., 2002; Finetti, 2005) or as an African promontory (e.g. Channell et al., 1979). The Adriatic Sea trends NW-SE with shallow bathymetry (<300 m) and sedimentary supply from the surrounding chains.

In the last twenties, several works have been devoted to investigate the shallow and deep crustal setting of the Central Adriatic, by producing different and, in part, contrasting geological and/or geophysical models (e.g. Argnani et al., 1993; Bertotti et al., 2001; Scrocca et al., 2005; Venisti et al., 2005; Finetti and Del Ben, 2005; Geletti et al., 2008; Scisciani and Calamita, 2009; Fantoni and Franciosi, 2010; Mancinelli et al., 2015; Pace et al., 2015; Mancinelli et al., 2018; Pauselli et al., 2019). Often, the adopted methods relied on the interpretation of seismic reflection or refraction profiles constrained by borehole data where available, to investigate geometries of upper crustal bodies. One of the key steps in working with seismic profiles is represented by the velocity model used to convert two-way time (TWT) to depth and properly support the retrieved model (e.g. Amadori et al., 2019). The velocity values of the modeled units, together with derived density values, are often inferred from sonic logs (e.g. Bigi et al., 2011; Montone and Mariucci, 2015, 2020) and used to support 2D and 3D geological or geophysical models across Central Italy (e.g. Porreca et al., 2018; Mancinelli et al., 2019, 2020).

In the central Adriatic, Plio-Quaternary (PQ) deposits may reach up to 9 km in thickness (Bigi et al., 1990) implying that their P-wave velocities have a significant influence on the depth conversion and restoration of geometries of the deeper crustal volumes from seismic profiles (e.g. Mancinelli et al., 2018). Moreover, the PQ deposits play a key-role in understanding the tectonic and geodynamic evolution of the Adriatic foreland basin and the adjacent Apennine fold-and-thrust belt in the last ~5 Ma. Plio-Pleistocene siliciclastic turbidites are the main reservoir for the shallow biogenic gas, that was largely explored in the Adriatic and Po-Plain basins (Bertello et al., 2010). In this context, is fundamental to investigate variations in pore pressure and eventual overpressure to provide valuable constraints for the evaluation of traps integrity (e.g. Lupa et al., 2002) and for possible future drilling activities (e.g. Mouchet and Mitchell, 1989). Further implication of pore pressure deviations derived from velocity are also relevant to provide constraints to fault mechanics, fault kinematic models (e.g. Tobin

* Corresponding author.
E-mail address: paolo.mancinelli@unich.it (P. Mancinelli)

https://doi.org/10.1016/j.marpetgeo.2020.104554
Received 25 April 2020; Received in revised form 19 June 2020; Accepted 21 June 2020
Available online xxx
0264-8172/

and Saffer, 2009) and define potential seismic or aseismic layers in the sedimentary cover (Hubbert and Rubey, 1959; Sibson, 1981).

Often targeted by exploration interests, in young foreland systems such as the Adriatic, time-depth relations from check-shot or Vertical Seismic Profiles (VSP) are rarely available. Reprocessed or 3D seismic profiles are similarly restricted, while the publicly-available well logs are often incomplete for the infilling units. Under this scenario of limited data availability, the models involving foredeep infilling were rarely supported by detailed velocity models.

In this work we integrate the interpretation of reprocessed seismic reflection profiles with previously unpublished data from boreholes to provide the first constrained velocity-depth relation for the Pliocene-Quaternary deposits in the Adriatic foreland. Results will contribute to reconstruct the geometry of the Apennines foredeep basin and, in the general understanding, of the parameters controlling velocity-depth trends within siliciclastic turbiditic (sandy and shaly) foreland succession. Moreover, we locate possible overpressures in the PQ deposits within the depth range of 2500–3500 m.

2. Geologic framework

The structural setting of the Adriatic sea was investigated through industrial hydrocarbon exploration 2D seismic reflection profiles and wells, together with deep-crust reflection seismic profiles of the CROsta Profonda (CROP) project (CROP Atlas, 2003), respectively recorded up to about 5.0 and 17.0 s in TWT (Fig. 1). The results of these investigations allowed to reconstruct (e.g. Bally et al., 1986; Malinverno and Ryan, 1986; Vai, 2001; Finetti and Del Ben, 2005; Scisciani and Calamita, 2009; Cazzini et al., 2015; Pace et al., 2015; Scisciani and Esestime, 2017 and references therein) a tectonostratigraphic evolution characterized by a Tethyan rift-related extensional tectonic phase starting from Late Permian and followed in the Late Triassic by the deposition of a thick interval of dolomites and evaporites of the Burano formation. The subsequent wide carbonate platform (Calcare Massiccio fm.), that developed during Early Jurassic was dismembered by the Jurassic rifting, with creation of pelagic carbonate basins separated by persisting shallow-water carbonate platforms. Starting from late Cretaceous, due to changes in the stress regime and erosion of the growing Alpine and Dinaric orogens, the main pelagic carbonate deposition was progressively replaced by a more terrigenous fraction, with marls and shales prevailing from early Paleogene (Scaglia group) to late Miocene (Bisciaro and Schlier formations). In the latest Miocene, the salinity crisis triggered the deposition of the Messinian Gessoso Solfifera evaporitic sequence before the onset of a new compressive phase related to the Apenninic orogenesis. This phase, lasting since Pliocene, produced the Central Adriatic foreland flexure in front of the E-NE-verging Apennine chain and the deposition of a thick wedge-shaped Plio-Quaternary foredeep infill (Pace et al., 2011; Scisciani and Montefalcone, 2006).

In the Adriatic foreland, the PQ turbiditic succession shows significant lateral heterogeneity in terms of thickness (e.g. Bigi et al., 1990; Scisciani and Esestime, 2017) and facies. The turbiditic sequences consist mainly of shales, representing source rocks and seals for the biogenic gas in the interbedded reservoirs, consisting of sandy and more rarely sandstones levels. Organic matter is of terrestrial origin and traps are mostly structural, related to Pliocene-Quaternary folds and thrusts (Fig. 1b) affecting the Adriatic foreland (Cazzini et al., 2015). Locally, the thickness of PQ deposits is controlled by faulting and folding, producing significant lateral variations (e.g. Bigi et al., 1990; Pace et al., 2015; Mancinelli et al., 2018). Despite the PQ represents one of the most attractive regions in southern Europe for gas production and storage (Cazzini et al., 2015), publicly-available well logs often report logged information only in its deepest parts.

The most prominent structure in the Central Adriatic sea is represented by the Mid Adriatic Ridge (MAR) (Fig. 1b), a NW-SE alignment of compressive structures (Finetti, 1982). The origin of the MAR is still debated in literature. In fact, some authors interpret the MAR as an intraplate deformation related to inversion tectonics (e.g. Argnani et al., 1993; Boccaletti et al., 2005; Scisciani, 2009), a view supported by inversion structures in the area of the Clara and Emma wells (Pace et al., 2015). De Alteriis (1995) proposed the MAR to be related to bulging of the Adriatic lithosphere, whereas other authors support the hypothesis of the MAR representing the frontal propagation of the Apenninic (e.g. Scrocca, 2006) or Dinaric (e.g. Finetti and Del Ben, 2005) thrust front, emphasized by diapric structures from the Triassic Burano salt (Geletti et al., 2008).

3. Data and methods

The publicly available data catalogue, hosted by the Italian Ministry of Economic Development VIDEPI (www.videpi.com), encompass over 2300 well logs and several thousands of km of seismic reflection profiles. These data were acquired since '60 to evaluate hydrocarbon potential over onshore and offshore regions pertaining to Italy. In 2011, some of the offshore seismic lines were reprocessed by a geophysical company (i.e., the former Spectrum Asa, TGS at present) to improve quality of the original data and evaluate new plays for oil and gas industry. These reprocessed data cover the Central and Southern Adriatic Sea, the so-called B (Fig. 1a) and F explorative zones, respectively; the adopted reprocessing techniques, together with comparison with original data, are discussed in Peace et al. (2012).

To investigate the zone B in Central Adriatic Sea (Fig. 1), we integrated over 8500 km of confidential reprocessed 2D seismic data and 88 available well logs from the VIDEPI catalogue, spanning from the northernmost well (Carmela_001), located 386775.7 E, 4886232.0 N (WGS84 UTM 33N), to the Gargano promontory with the southernmost well (Elizabeth_001), located 496544.3 E, 4653016.7 N (WGS84 UTM 33N).

3.1. Time-isochore maps from reprocessed seismic data interpretation

The seismic grid has an irregular spacing ranging between 7 and 25 km, while boreholes are irregularly distributed across the study area and often are located above anticlines (Fig. 1). Together with the publicly-available information retrievable from well logs, we also analyzed time-depth data from boreholes (check-shot and Vertical Seismic Profiles (VSP) survey data), partially integrated with sonic-log based data (i.e. interval velocities calculated from decimated interval transit times data), from 20 wells located within the B zone.

To focus on the Apenninic foredeep basin physiography and Plio-Quaternary basin infill, we interpreted the base of the Plio-Quaternary deposits (BPQ) and the sea-bottom (SB) reflectors (Fig. 2). The BPQ reflector is the most prominent and coherent reflection in the Adriatic basin and this feature makes its interpretation more confident also with scattered or in absence of borehole constraints. This signal originates along the interface between the "slow" fine-grained (mainly shales or marls) sediments and the "fast" evaporites of the Messinian Gessoso-Solfifera formation. The resulting high-amplitude and low-frequency BPQ reflector originated from the hard-kick (a trough in 'SEG reverse' polarity) is laterally continuous and easy to correlate throughout the entire 2D seismic dataset (Fig. 2). The BPQ reflection continuity is locally interrupted by channels and unconformities that truncate the Messinian evaporites and along which the Pliocene-Quaternary deposits are directly juxtaposed onto Miocene-Cretaceous marls and carbonates (Fig. 2), still generating an hard-kick. This approach was chosen to map the top BPQ, independently from well data and introducing the minimum amount of doubt in the interpretation.

Starting from well-tie to seismic and by using a loop-tying correlation of the two reflectors respectively at the top and base of the Plio-Quaternary succession, we produced the TWT contour map of the sea-

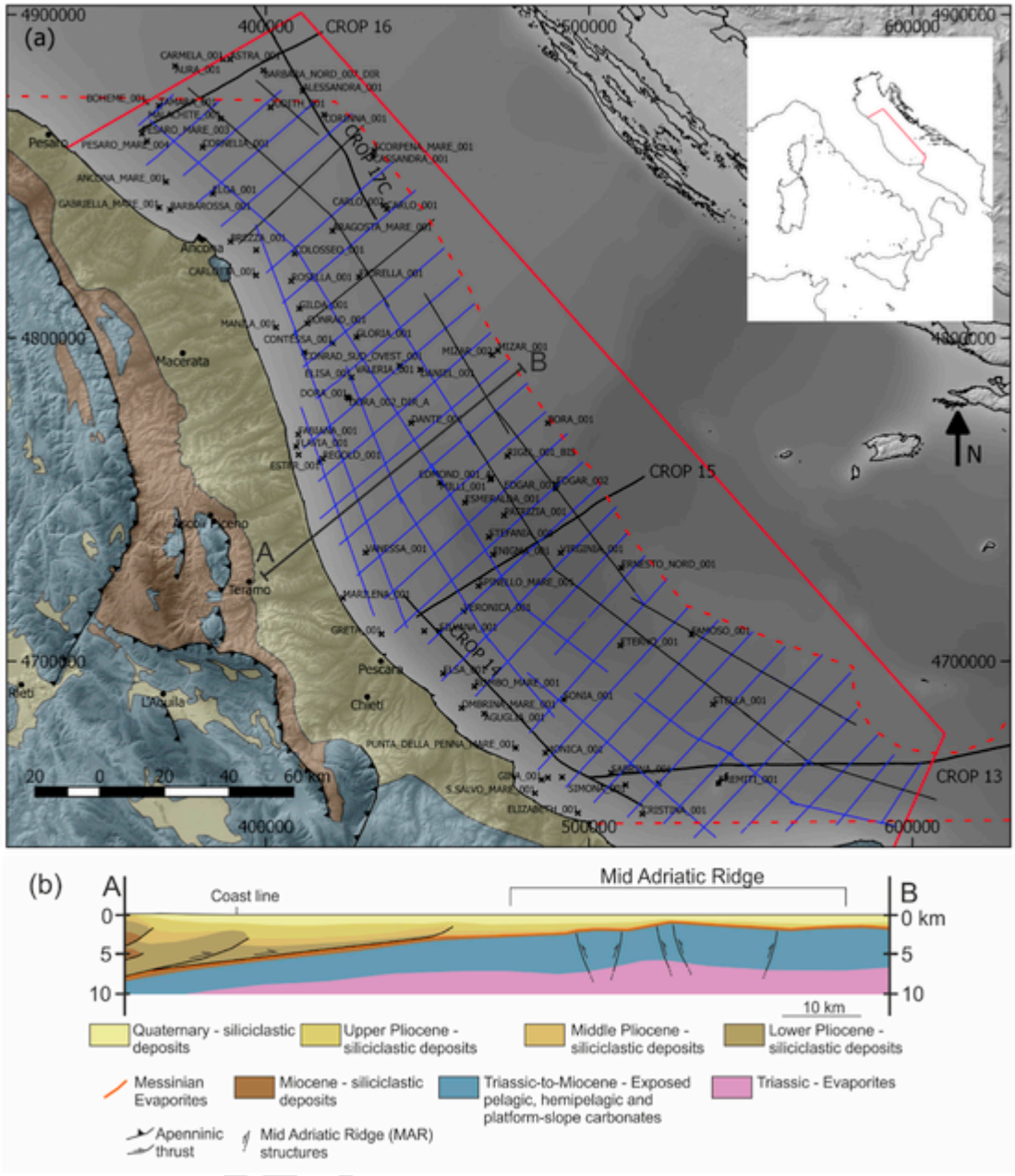

Fig. 1. (a) Geological sketch map of the study area (red continuous polygon) with location of the analyzed seismic lines and wells. Red dashed polygon locates the ministerial zone B in the Central Adriatic. Crosses indicate the available well logs from VIDEPI. Blue lines locate the reprocessed seismic lines, black thin lines indicate the original seismic profiles (not reprocessed) and thick black lines locate the CROP profiles. (b) Schematic geological cross-section across the study area (modified from Scisciani and Calamita, 2009). Stratigraphic ages refer to the period in which well logs were compiled (i.e. mid '60s to late '90s). Basemap topography in this and following figures ranges between 2912 and 0 m a.s.l. and is from Tarquini et al. (2007, 2012). Coordinates in all figures are in WGS84 UTM 33N. (For interpretation of the references to colour in this figure legend, the reader is referred to the Web version of this article.)

bottom (Fig. 3a) and of BPQ (Fig. 3b), confidently traced across all CROP and industrial seismic profiles. By difference between the two surfaces we can easily compute the TWT thickness of the PQ deposits (Fig. 3c).

The map of the TWT contour lines of BPQ (Fig. 3b) is comparable to the TWT thickness of the PQ (Fig. 3c) due to the limited bathymetry of the Adriatic Sea (Fig. 3a). Showing a general NE-ward decreasing trend, the TWT thickness of the PQ succession ranges from values of ~0 s, toward south, to values of over 4 s near the shoreline in the central portion of the study area with ~20 km-wide local oscillations observable in the central part of zone B. In particular, dashed black lines in Fig. 3c report an alignment of local minima (<0.8 s) often not related to major faults affecting the PQ deposits.

3.2. PQ thickness from well data

Explorative wells in the B zone were drilled since '60 to evaluate possible hydrocarbon prospects identified after seismic profiles acquisition and interpretation. When targeted to specific deep units beneath the BPQ, the logging was often started in Pliocene deposits, whereas if the explorative target was in PQ deposits the drilling and logging was limited to post-Messinian units. For these reasons, in the study area and immediate surroundings, only 53 of the available 88 wells (Fig. 1) are

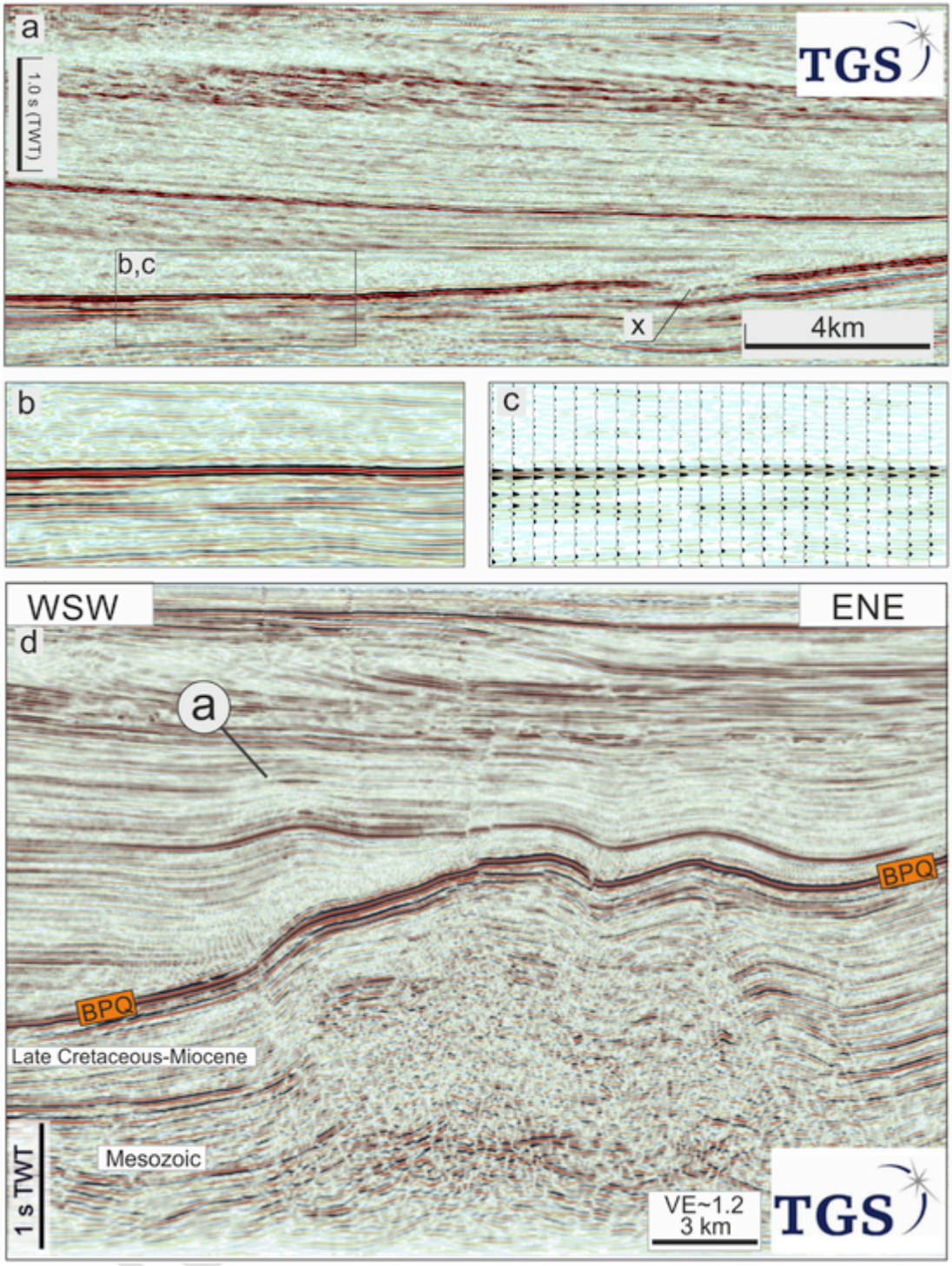

Fig. 2. a) Seismic profile showing the prominent BPQ reflector at the base of the Plio-Quaternary deposits; the lateral continuity of the BPQ reflector is interrupted by local channels (X) or unconformities. b) Typical aspect of the high-amplitude and low-frequency BPQ reflector (trough in 'SEG reverse' polarity) originated at the interface between the "slow" fine-grained (mainly shales or marls) sediments and "fast" Messinian evaporites (downward kick); c) Colored amplitude overlaid by a black and white display of the wiggle trace showing the prominent trough of the waveform along the BPQ reflector in 'SEG reverse' polarity (trough = downward increase in acoustic impedance). d) Seismic profile showing the typical style of the compressive structures within the Mid Adriatic Ridge. Top of figures (a) and (d) is close to the sea level. Note the prominent flat spot (a) produced by the biogenic gas in the culmination of an anticline affecting the Pliocene foredeep deposits (modified from Pace et al., 2015).

used in this work, because these only drilled the BPQ and provide reliable constraints on the thickness of the Pliocene and Quaternary deposits. From the well logs, we collected the thickness of the PQ deposits – i.e. the thickness between BPQ and sea-bottom (Fig. 4), together with information about eventual fluid content (water and salt water, fluid hydrocarbons) in PQ deposits (Table 1).

The thickness of PQ deposits retrieved from well logs shows a general WSW-increasing trend, in agreement with the Apenninic foreland deepening toward the Italian shoreline, with maximum thickness observed in the Silvana (3410.3 m) and Elsa (3021 m) wells in the B1 region of the study area (Fig. 4). However, some local variations are ob-

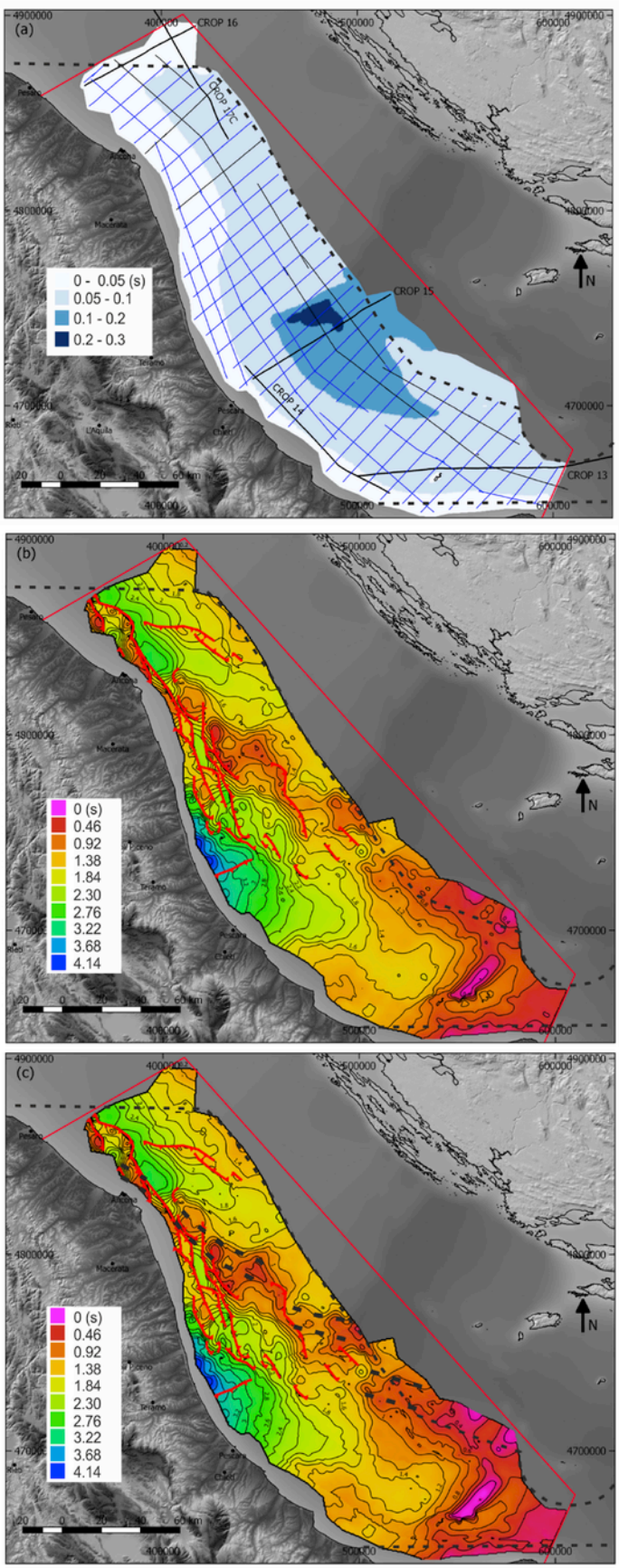

Fig. 3. (a) TWT map of the sea-bottom, locations of seismic lines are shown as in Fig. 1. (b) TWT contour map of the BPQ. (c) TWT thickness map of the PQ deposits. Thin black dashed polygon locates the ministerial zone B in the Central Adriatic Sea. Bold red lines in (b) and (c) locate main faults affecting the base of Plio-Quaternary deposits. Color scale and contour spacing (0.2 s) in (b) and (c) are the same. Bold dashed lines in (c) locate trend of PQ local minima thickness. (For interpretation of the references to colour in this figure legend, the reader is referred to the Web version of this article.)

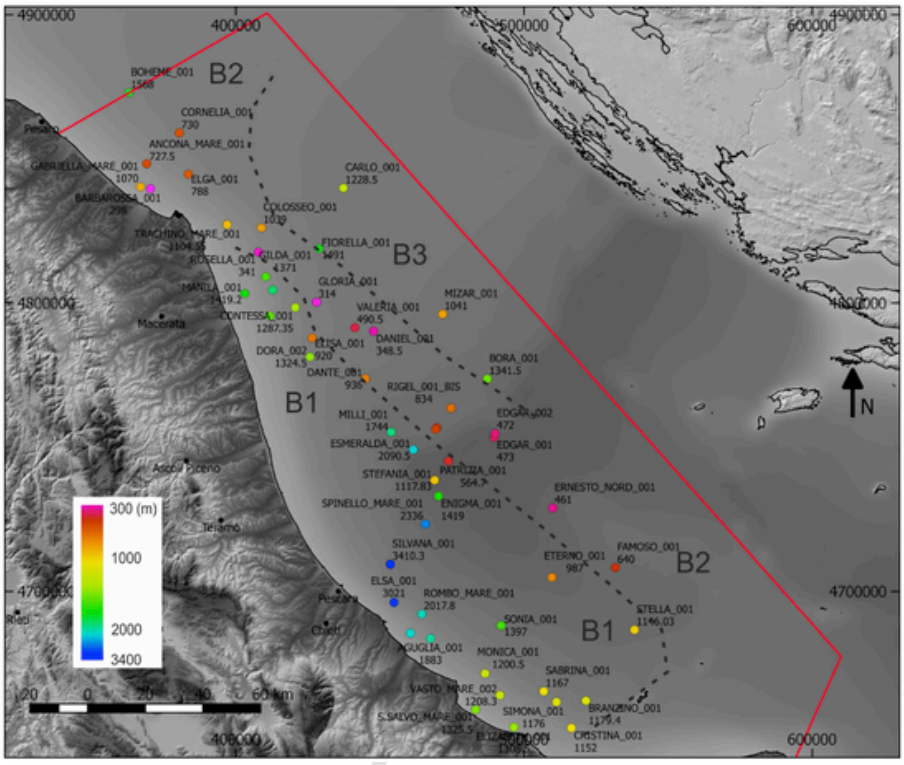

Fig. 4. Thickness of the PQ deposits from 53 well logs across the study area (red polygon). Values within labels show the PQ thickness in meters. Black dashed lines locate boundaries between regions (B1–B3) with similar thickness of PQ deposits. (For interpretation of the references to colour in this figure legend, the reader is referred to the Web version of this article.)

served. In particular, a NW-SE alignment of wells reporting low PQ thickness values is observed from the northernmost Barbarossa well (298 m) to the southernmost Famoso (640 m) well in the B2 region of the study area. This alignment corresponds to the spatial distribution of the TWT minima observed in Fig. 3c and will be discussed in section 4.1. The thickness of the PQ deposits tends to increase NE of this alignment, in the B3 region of the study area (Fig. 4).

3.3. TWT thickness from time-depth data

Logs available in the VIDEPI dataset generally plot the spontaneous potential, resistivity, sonic velocity and total gas, together with microfossil content, estimated age and lithology. However, for some wells located within the study area, we have also information about one way time (OWT) arrivals from time-depth data (Fig. 5). These data have been interpolated with a second-order polynomial fit in Fig. 5, representing the estimated time-depth trend for the PQ deposits. In Fig. 5, the red line represents the best-fitting interpolation of the OWT trend with depth and provides a correlation coefficient R^2 of 0.98 and a root-mean-square-error (RMSE) of 0.045. Similarly, the interpolation of the depth from the OWT by reverting the previous equation, provides a good fit with an R^2 of 0.99 and a RMSE of 116.5. Interestingly, OWT arrivals from boreholes located in the area with thicker PQ deposits (region B1 in Fig. 4) are relatively faster – i.e. show smaller OWT, than data from wells in the B2 region (Fig. 5).

To test the validity of the OWT interpolation function across the entire study area, we used this function to convert thickness values of PQ retrieved from well logs (Table 1, Fig. 4) in TWT thickness (TWT = 2 OWT). This step was performed with the reasonable assumption that the TWT thickness of the PQ deposits from the seismic dataset, once removed the TWT thickness of seawater (Fig. 3c), is comparable to the thickness logged by boreholes and converted in TWT using the interpolation function from Fig. 5.

We sampled the TWT thickness map from seismic data (Fig. 3c) at the 44 boreholes whose locations within the B zone allowed to attribute a TWT value (Table 1). Finally, we compare this reference value with the thickness from well logs and converted in TWT, after interpolation of time-depth data from boreholes. This step was carried out considering the TWT value derived from the seismic grid interpretation as a reference value to test the goodness of the interpolation across the entire Central Adriatic.

Fig. 6a shows the percentage values of the TWT thickness from seismic data that is estimated by the interpolating function retrieved from time-depth data. In this map, values over 100 locate wells where the function over-estimates the TWT thickness, while values below 100 locate wells with under-estimated PQ TWT thickness. In Fig. 6b we compare data from well logs and seismic grid interpretation with TWT thickness estimates on three sample wells. In this figure Tc values denote the calculated TWT thickness of PQ (Fig. 3c) at well location, while Te values denote the TWT PQ thickness estimated using the OWT interpolating function from time-depth data (Fig. 5) and calculated using the PQ thickness as reported in well logs.

4. Results and discussion

4.1. Discussion of plots and maps

The comparison of TWT thickness map of PQ deposits after seismic data interpretation (Fig. 3c) with thickness values retrieved from well

Table 1
Wells with retrieved thickness of PQ deposits, logged interval in public log and logged mineralization type and interval. The 44 wells with TWT thickness data (some wells are not covered by the used seismic dataset) show the value retrieved from the PQ TWT thickness map obtained from the seismic dataset (Fig. 3c). Ages of levels with hydrocarbons are referred to the original well logs compilation. Coordinates are in WGS84 UTM 33N. Well logs are available at https://www.videpi.com/videpi/pozzi/consultabili.asp.

Well Name	X (m)	Y (m)	Pliocene-Quaternary thickness (m)	TWT thickness from seismic (s)	Fluid Content	Logged Total Gas?	Epoch of deposits with hydrocarbons
AGUGLIA_001	467563.9	4683762	1883	–	GAS	YES	PLIOCENE + PLEISTO
ANCONA MARE_001	369120	4848286	727.5	–	NONE	NO	
BARBAROSSA_001	370398.5	4839610	298	–	NOT CLEAR	NOT CLEAR	
BOHEME_001	362968.3	4872976	1568	–	NONE	NO	
BORA_001	487255.25	4773648.4	1341.5	1.4212	NOT CLEAR	NOT CLEAR	
BRANZINO_001	521515.88	4662218.4	1179.4	1.1321	GAS	YES	
CARLO_001	437391.71	4839895.8	1228.5	1.3339	SALT WATER	NO	
COLOSSEO_001	408932.51	4826098	1039	1.1269	NONE	NO	
CONRAD_001	412813.73	4804482.7	1641.55	1.4597	SALT WATER	NO	
CONRAD_SUD_OVEST_001	411882.49	4795499.6	1350.2	1.3928	WATER + SALT WATER	NO	
CONTESSA_001	420663.12	4798416	1287.35	1.6074	NONE	NO	
CORNELIA_001	380438.51	4859016.3	730	0.855	NONE	NO	
CRISTINA_001	516476.45	4652756.1	1152	1.155	WATER + SALT WATER	YES	
DANIEL_001	447799.37	4790211.9	348.5	0.5376	NONE	NO	
DANTE_001	444954.21	4773727.1	936	1.3169	GAS	YES	PLEISTOCENE
DORA_002	425730.1	4781299.8	1015.5	1.2193	GAS	YES	UPP PLIO + PLE
EDGAR_001	489703.61	4753361.6	473	0.5976	NONE	NO	
EDGAR_002	489945.89	4754690.3	472	0.6249	NONE	NO	
EDMOND_001_A	469770.02	4756674.3	651	0.9203	NONE	YES	
EDMOND_001_TER	469396.24	4756161.8	672	0.969	NONE	NO	
ELGA_001	383561.41	4844678.9	788	0.9444	NONE	NO	
ELISA_001	426496.34	4787858.1	920	0.9981	NONE	NO	
ELIZABETH_001	496544.3	4653017	1308.5	–	GAS	YES	PLIOCENE + PLEISTO
ELSA_001	454890.73	4696197	3021	2.3157	GAS	YES	PLIOCENE + PLEISTO
ENIGMA_001	470349.48	4732976.3	1419	1.4548	GAS	YES	UPP PLIO + PLE
ERNESTO_NORD_001	509972.47	4728864.9	461	0.7121	NONE	NO	
ESMERALDA_001	461607.32	4749082.5	2090.5	2.0404	GAS	YES	UPP PLIO + PLE
ETERNO_001	509700.78	4704859	987	1.1153	GAS	YES	PLEISTOCENE
FAMOSO_001	531723.48	4708246.9	640	0.6862	NONE	YES	
FIORELLA_001	428860.31	4818841.2	1491	1.6187	GAS	YES	PLIOCENE + PLEISTO
GABRIELLA MARE_001	366970.7	4840304	1070	–	NONE	NO	
GILDA_001	410373.58	4809086.3	1371	1.461	SALT WATER	YES	
GLORIA_001	428055.12	4800254.5	314	0.4148	NONE	NO	
MANILA_001	403124.6	4803263	1419.2	–	WATER	NO	
MILLI_001	453913.78	4755184.6	1744	1.6798	NONE	NO	
MIZAR_001	471793.74	4796128.3	1041	1.3401	SALT WATER	NO	
MONICA_001	486526.74	4671609	1200.5	1.1405	NONE	YES	
OMBRINA MARE_001	460580.1	4685520	2027	–	GAS	YES	PLIOCENE + PLEISTO
PATRIZIA_001	473743.16	4745097.4	564.7	1.1314	WATER + GAS	YES	PLEISTOCENE
RIGEL_001_BIS	474724.91	4763511.5	834	0.8828	NONE	YES	
ROMBO_MARE_001	464554.72	4692157.7	2017.8	1.7067	NONE	NOT CLEAR	
ROSELLA_001	407889.19	4817630.3	341	0.46	NONE	NO	
S.SALVO MARE_001	483264.4	4659128	1325.5	–	NONE	NO	
SABRINA_001	506851.58	4665457.7	1167	1.1698	GAS	YES	UPP PLIO + PLE
SILVANA_001	453639.81	4709383.5	3410.3	2.5996	GAS	YES	UPP PLIO + PLE
SIMONA_001	511275.53	4661740.6	1176	1.1935	GAS	YES	PLEISTOCENE
SONIA_001	492119.36	4688195.8	1397	1.2876	GAS IN LEVELS	YES	UPP PLIO + PLE
SPINELLO_MARE_001	465800.16	4723265.8	2336	2.0251	GAS	YES	UPP PLIO + PLE
STEFANIA_001	469005.72	4738478.2	1117.83	1.3802	SALT WATER	NO	
STELLA_001	538358.79	4686683.3	1146.03	1.1881	NOT CLEAR	NO	
TRACHINO_MARE_001	397027.73	4827163.6	1104.55	1.08	GAS	YES	UPP PLIO + PLE
VALERIA_001	441332.47	4791412.2	490.5	0.6376	NONE	NO	
VASTO_MARE_002	491657.27	4664107.9	1208.3	1.2174	NONE	YES	

logs (Fig. 4), highlights a general matching between the two datasets. Given the extent and spacing of the seismic grid, we consider the spatial trend from TWT maps (Fig. 3c) to be more representative than punctual information from wells. Finally, considering the NW-SE trend of the observed relative minima, we interpret these values as mostly representative of the Mid Adriatic Ridge (MAR) with possible local con-

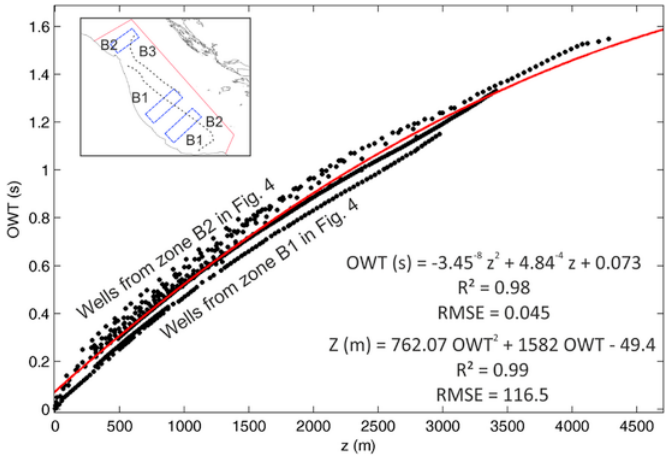

Fig. 5. OWT arrivals at corresponding depths (z) from borehole data. Red line interpolates the data with a second-order polynomial fit described by the equation on the right. Blue squares in the inset map show the locations of the boreholes used in this plot. Data from boreholes in the B1 region (Fig. 4) locate below the red line, while data from boreholes in the B2 region locate above. In the equations for OWT(s) and z(m), R^2 is the correlation coefficient, RMSE is the root-mean-square-error. (For interpretation of the references to colour in this figure legend, the reader is referred to the Web version of this article.)

tributions from fault-related folds affecting the PQ deposits. In fact, the MAR consists of several N-S to NW-SE oriented anticlines related to deep blind faults (Fig. 2d in this work and Fig. 11 in Pace et al., 2015); these reverse to transpressive structures commonly reactivated inherited Mesozoic normal faults in an inversion tectonic context (Scisciani, 2009; Pace et al., 2015; Scisciani et al., 2019; Tavarnelli et al., 2019). The growth of the MAR anticlines occurred mostly during Pliocene and early Pleistocene, confining to the NE the deposition and north-sourced Lower Pliocene turbidites (Cellino Fm. – Casnedi, 1983; Dattilo et al., 1999). Consequently, the early Pliocene thick-bedded sandstone are restricted into the NNW-SSE trending depocentral axis of the Adriatic foredeep and are replaced by prevailing shales on top of the growing MAR anticlines (Finetti et al., 2005; Scisciani et al., 2010). During late Pliocene and early Pleistocene, an acceleration of the tectonic subsidence affected the Adriatic foredeep (Scisciani and Montefalcone, 2006; Artoni, 2013; Mancinelli et al., 2018) producing a NE-ward expansion of the former foredeep basin with drowning of the MAR structures and the shifting of the depocenter and of the coarse grained turbidite system infill. During the Late Pliocene and early Pleistocene, low-efficiency turbiditic systems, still fed from NNW, were sedimented onto the subsiding MAR. The subsequent deformation of these thin-bedded sandy reservoirs produced significant trapping for the biogenic gas.

If we assume that the OWT data may represent a first approximation of the inversely proportional bulk seismic velocity for the PQ deposits, their distribution (Fig. 5) suggests that, within the foredeep, some changes must occur if the interpolation is considered as a reference average value. In fact, we report a decrease of OWT arrivals – i.e. an increase of velocity, for wells located near the foredeep depocenter (B1 region in Fig. 4) while OWTs increase if wells in central Adriatic are considered (B2 region in Fig. 4). We interpret this trend as representative of lithological changes from more proximal facies in the B1 region, close to the Apenninic chain, to more distal deposits away from the chain (Fig. 1).

Integration of TWT maps with borehole data allowed us to test across the entire study area the interpolating function retrieved from boreholes time-depth data. In fact, the comparison of these two independent values of PQ TWT thickness, highlights a general fit between values predicted by the time-depth relation provided in Fig. 5 and the TWT maps after seismic profiles interpretation.

Noteworthy, TWT values are under- or over-estimated by values exceeding ±20% only in two locations – i.e. Patrizia_001 and Dante_001 wells (red triangles in Fig. 6a). In all other wells the estimation produces values within the ±20% range if compared to TWT obtained from seismic grid, with the only exceptions located in seven wells (orange points in Fig. 6a) where 10–18% under-estimation occurs. Wells with the larger under-estimated values (orange and red points in Fig. 6a) align NW-SE, while wells with higher over-estimations (blue points in Fig. 6a) are mostly located in the south, where higher thicknesses of PQ deposits were found (Fig. 4).

Considering the quality of the seismic grid (Fig. 2), the time-depth data (Fig. 5) and the reliability of well logs – i.e. the input values used so far, it is sounding to assume that these variations in terms of estimated values and of their spatial distribution should be addressed to local changes of the time-depth relation within the PQ deposits rather than to the proposed time-depth relation retrieved from boreholes.

Analogously to bulk velocity changes observed from OWT data, the parameters affecting the possible time-depth behavior of sands and shales constituting the PQ deposits may be grouped in two major contributors: compaction and fluid content. The first is directly related to burial, porosity and lithology (i.e. shale content) while the second is related to the eventuality that gas, oil or water may be trapped in pores. Unfortunately, the available well logs do not show porosity data of the drilled deposits but in some wells the gas content and mineralization type are logged (Table 1).

We note that among the wells with larger mismatches in Fig. 6, fluids within PQ deposits are reported on several logs (triangles in Fig. 6a), with logged total gas content locally exceeding 10% (e.g. Dante_001 well) or even 50% (e.g. Dora_002 well). Thus, we can speculate that at least a portion of the observed mismatch on predicted TWT can be related to fluid content of PQ deposits. Some contribution from porosity and local lithological changes may be present but, at the current state of knowledge, is hard to quantify. However, it should be noted that half of the wells in zone B do not report the total gas log on published data (Table 1), but this does not imply that gas or water content in those PQ deposits is null.

4.2. Velocity plots

Once tested the reliability of the OWT-depth fit across the entire B zone, we compute the depth trend of the seismic velocity (V_P) of PQ deposits within depth windows ≤ 100 m and refer the calculated velocity value to the central point between the two measured points. Fig. 7a shows the obtained V_P-depth trend. Within this plot we also report linear and exponential fit over the data. These fitting functions were derived from equations proposed in literature for sand-shale sequences (Faust, 1951; Acheson, 1963; Slotnik, 1936; Bulat and Stoker, 1987; Japsen et al., 2007). In Fig. 7b we also show residuals plot for both interpolations. The resulting dataset comprise over 700 data points with velocity values ranging between 1500 and 3800 m/s and an average velocity across the entire depth of ~2650 m/s, values similar to the North Sea sandstones and shales (Avseth et al., 2001).

The linear fit provides a V_0 value of 1849 (m/s) with a velocity-depth gradient k of 0.51, while the exponential interpolator results in a coefficient c of 433 and a corrective factor for the exponent n of 0.748, slightly below the range proposed by Japsen et al. (2007 and references therein).

Fitting of the V_P-depth plot provides good results both considering a linear or exponential interpolation. In particular, both interpolations provide similar R^2 and RMSE values, slightly better for the exponential. This result is in agreement with velocity-depth relations proposed for sand-shale sequences (Faust, 1951; Acheson, 1963; Japsen et al.,

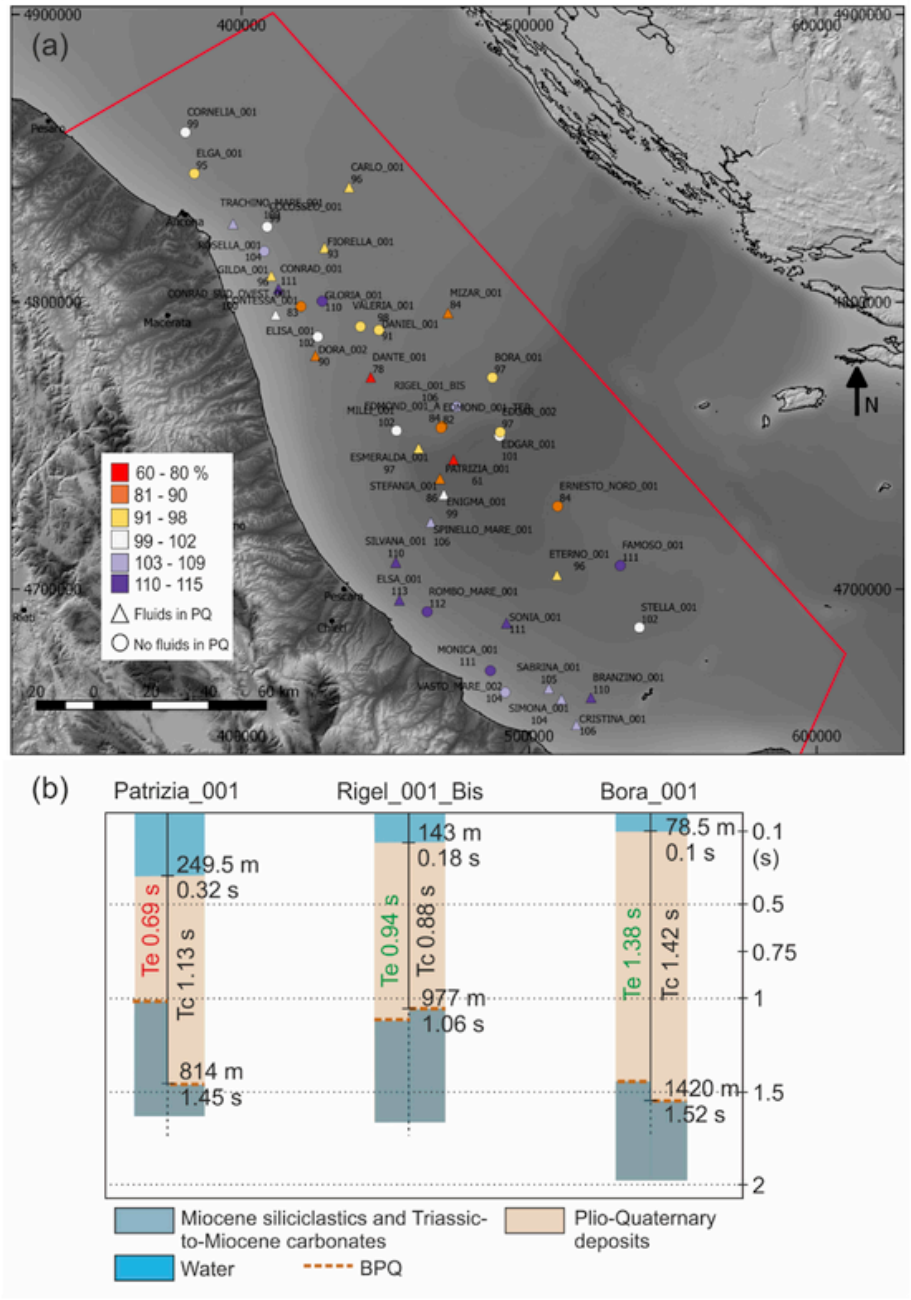

Fig. 6. (a) Estimate of the percentage deviation of the TWT thickness of PQ deposits by the interpolating function retrieved from time-depth data taking as reference value the TWT thickness from seismic profiles interpretation sampled at well locations. Values over 100 locate points where the function derived in Fig. 5 over-estimates the TWT thickness. Values below 100 locate points where under-estimation occurs. Triangles and circles respectively locate wells with or without log-reported water and/or gas in PQ deposits. (b) Comparison between three wells: the data retrieved from well logs (depths) and maps after seismic interpretation (TWT) are in black in the right part of each column, while the estimated TWT thicknesses after Fig. 5 are reported in green (estimation error < 10%) or red (estimation error > 10%) in the left part of each column. Tc represents the TWT thickness of PQ calculated from seismic grid interpretation – i.e. TWT depth of BPQ minus TWT thickness of the water column. Te represents the estimated TWT thickness using the OWT interpolation in Fig. 5. (For interpretation of the references to colour in this figure legend, the reader is referred to the Web version of this article.)

2007) and shales from the Bavarian Molasse basin (Drews et al., 2018).

Residuals of the two fits show similar trends at depths between 500 and 3500 m, while they diverge at shallower or higher depths. Larger residual values – i.e. more scattered data points, are observed below 1500 m depth (Fig. 7b), for this reason in Fig. 8 we separately plot V_P values for depths between 0 and 1500 m.

In this case the best-fitting interpolation, both considering R^2 and RMSE, is provided by the linear fit (blue line in Fig. 8a) while range of residuals is obviously smaller than in the previous plot (Fig. 7b), due to the less scattered data.

Interestingly, the shallower deposits seem to fit well with a linear increase of velocity with depth like $V_P(z) = V_0 + k\,z$ while if a wider range of depths is taken – i.e. a range encompassing the entire PQ sequences, the best velocity-depth trend is provided with an exponential fit in the form of $V_P(z) = c\,z^{(1-n)}$.

Velocity data pertaining to the depth range between 2500 and 3500 m in Fig. 7 show anomalous changes if compared to linear or exponential normal trends. Within this depth range, two velocity anomaly

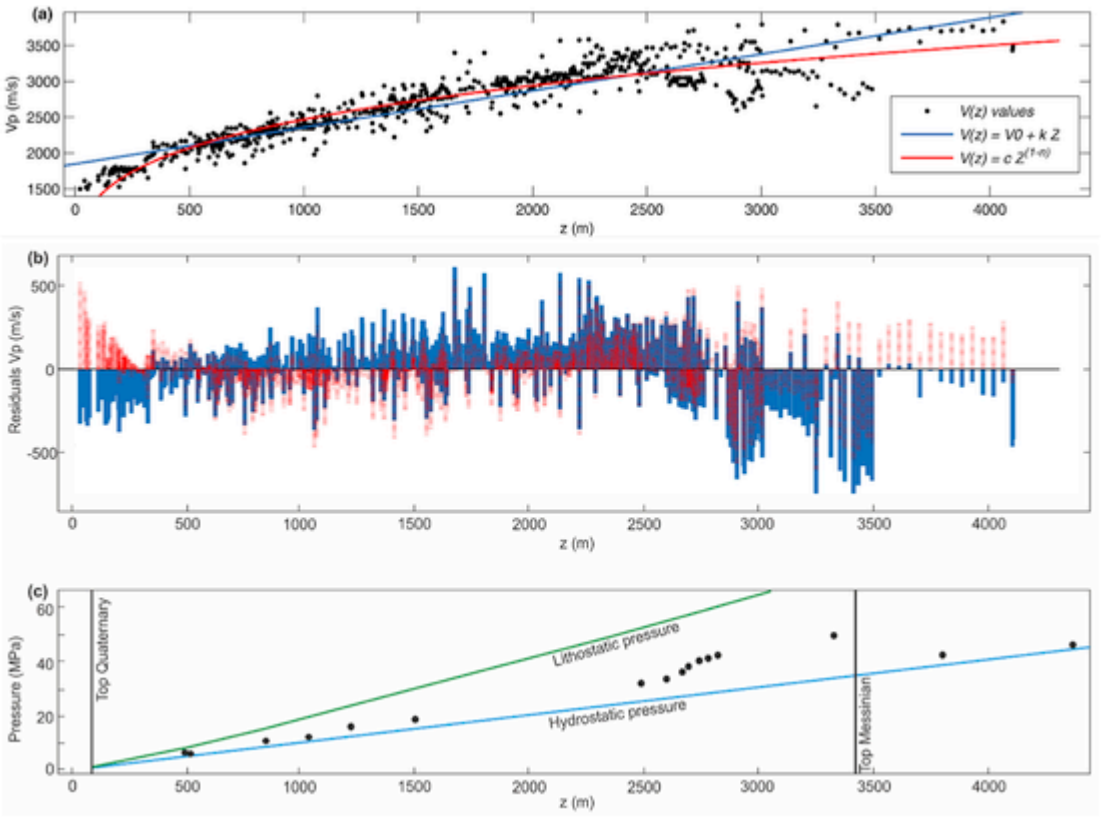

Fig. 7. (a) calculated V_P values fitted by linear (blue line) and exponential (red line) trends. (b) residual plots of the linear (blue vertical lines) and exponential (red vertical dashed lines) fitting functions. R^2 for linear fit is 0.83, RMSE is 215.7. R^2 for exponential fit is 0.86 and RMSE is 191.8. (c) formation-fluid pressure (dots) computed from mud density data in the Silvana 1 borehole. (For interpretation of the references to colour in this figure legend, the reader is referred to the Web version of this article.)

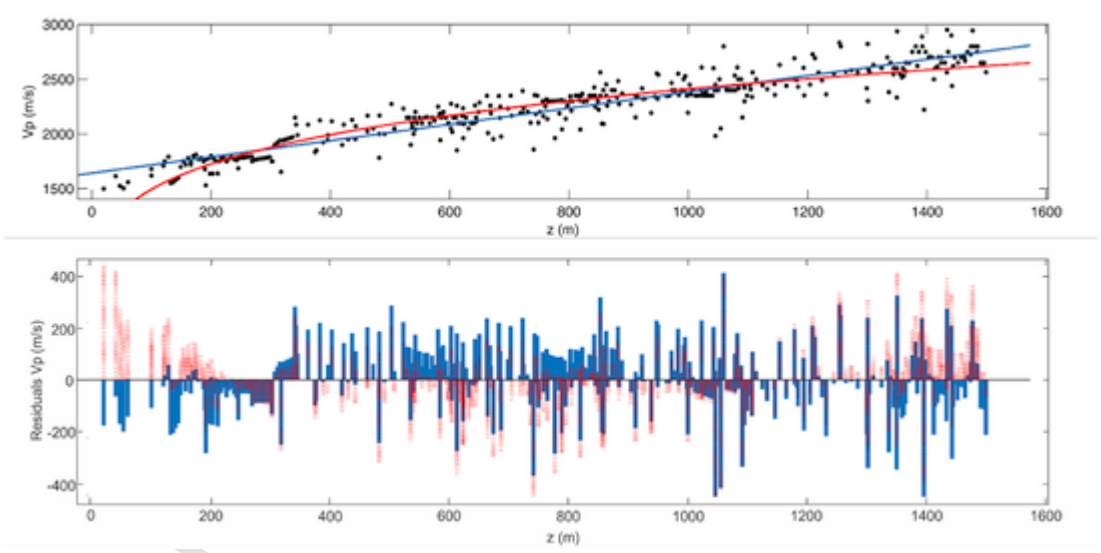

Fig. 8. Same plot as in Fig. 7 but limited to data points between 0 and 1500 m depth. Interpolations are produced with the same equations used in Fig. 7. Linear fit shows an R^2 of 0.86 and RMSE of 118.5, exponential fit has an R^2 of 0.85 and RMSE of 125.6.

cycles occur at 2500 and 3000 m depth, with a significant decrease of velocity values between 2500 and 3000 m and a rapid increase immediately below 3000 m. This is followed by another decrease between 3000 and 3500 m. These anomalies are clearly observable from velocity-depth plots (Fig. 7a), while velocity loss is estimated by residuals plot to be ~500 m/s (Fig. 7b).

These rapid velocity changes are similar to those observed in under-compacted over-pressured Cenozoic shales in the North Sea by Japsen (1999) and suggest a similar situation for these deep PQ deposits in Central Adriatic. Unfortunately, we lack in situ pressure measurements from boreholes about PQ or underlying deposits, but an estimate of formation-fluid pressure from mud density supports this interpretation (Fig. 7c). Moreover, the scenario of Pliocene shales that underwent a rapid burial in low-permeability conditions causing overpressure, fits the high sedimentation rates during Pliocene (Mancinelli et al., 2018). This observation, framed in a geodynamic phase that was domi-

nated by horizontal forces due to the Apenninic orogenesis, allows us to further stress that, in the evolution of foreland basins, the vertical contributions due to crustal flexure, sedimentation, burial (e.g. Drews et al., 2018; Mancinelli et al., 2018) and possibly subsidence accumulation due to other sources (e.g. Simpson, 2014 and references therein) play a significant role. Of course, the quantification of the contributions related to thrust propagation in the foredeep during the Pliocene, would certainly increase the level of detail and confidence about these overpressures. This should also require currently-unavailable 3D seismic volumes and full well logs for a detailed 3D kinematic modeling of the thrust fronts.

5. Conclusions

Based on reprocessed seismic profiles and unpublished borehole data, in this work we present V_P-depth relations for Pliocene-Quaternary (PQ) sands and shales in the Central Adriatic foredeep. We first convert thickness of the PQ deposits from boreholes in TWT and then compare these values with those retrieved from the interpretation of a dense grid of partially reprocessed seismic profiles. We discuss anomalies in the spatial trend of the PQ thickness and OWT data, by suggesting contributions from gas content and lithological variations to locally affect the predictive trend of the OWT-derived time-depth trend. This procedure validated the OWT-depth dataset across the entire central Adriatic sea, allowing to confidently use those data to retrieve a V_P-depth relation representative of the PQ deposits. We report that an exponential function in the form $V_P(z) = c\, z^{(1-n)}$ may fit data across the entire depth range. Anyway, at shallow depths (i.e. above 1500 m of depth), a linear function, like $V_P(z) = V_0 + k\, z$, may also confidently reflect velocity changes with depth. Velocity anomalies found between 2500 and 3500 m depth suggest overpressure of the PQ deposits triggered by compressive stress close to the Apenninic thrust front and the rapid burial history of the Pliocene deposits in Central Adriatic Sea. The retrieved velocity-depth functions represent a key step to refine the geometries of the Adriatic foredeep and underlying units, supporting geological and geophysical modeling and contributing to the general understanding of the foredeep systems. Furthermore, the proper definition of PQ velocity-depth trends and location of possible overpressured levels is fundamental to evaluate the seismogenic potential of the Adriatic foredeep and its capabilities in terms of oil and gas production and storage. Results of this work suggest that, whether the target is in the foredeep deposits or in the deeper units, the foreland basin modeling procedure should adopt measures to test across the entire volume the validity of the punctual information obtained from boreholes. Finally, the vertical variations of parameters like fluid content, lithology (sandy vs shaly turbidite content) and thickness of the infilling deposits, will certainly reflect changes in the evolution of the foreland and affect the velocity-depth relation with significant outcomes on the reliability of the retrieved models.

CRediT authorship contribution statement

Paolo Mancinelli: Conceptualization, Methodology, Writing - original draft. **Vittorio Scisciani:** Data curation, Methodology, Writing - original draft.

Declaration of competing interest

The authors declare that they have no known competing financial interests or personal relationships that could have appeared to influence the work reported in this paper.

Acknowledgements

We warmly acknowledge the insightful, constructive and detailed revisions of Giovanni Toscani and an anonymous reviewer. We thank TGS for granting the permission to publish the seismic data shown in Fig. 2; the seismic interpretation software was kindly provided by IHS Markit (Kingdom) and Schlumberger (Petrel). This work was supported by Chieti-Pescara University funds (to V. Scisciani and P. Mancinelli).

Appendix A. Supplementary data

Supplementary data to this article can be found online at https://doi.org/10.1016/j.marpetgeo.2020.104554.

References

Acheson, C H, 1963. Time-depth and velocity-depth relations in western Canada. Geophysics 28, 894–909.

Amadori, C, Toscani, G, Di Giulio, A, Maesano, F E, D'Ambrogi, C, Ghielmi, M, Fantoni, R, 2019. From cylindrical to non-cylindrical foreland basin: Pliocene–Pleistocene evolution of the Po Plain–Northern Adriatic basin (Italy). Basin Res. 31, 991–1015. doi:10.1111/bre.12369.

Argnani, A, Favali, P, Frugoni, F, Gasperini, M, Ligi, M, Marani, M, Mattietti, G, Mele, G, 1993. Foreland deformational pattern in the southern Adriatic sea. Ann. Geophys. 36, 229–247.

Artoni, A, 2013. The Pliocene-Pleistocene stratigraphic and tectonic evolution of the Central. Mar. Petrol. Geol. 42, 82–106.

Avseth, P, Mavko, G, Dvorkin, G, Mukerji, T, 2001. Rock physics and seismic properties of sands and shales as a function of burial depth. In: SEG int.L Exposition and Annual Meeting, San Antonio, Texas, September 9-14, 2001.

Bally, A W, Burbi, L, Cooper, C, Ghelardoni, R, 1986. Balanced sections and seismic reflection profiles across the Central Apennines. Mem. Soc. Geol. Ital. 35, 257–310.

Bertello, F, Fantoni, R, Franciosi, R, Gatti, V, Ghielmi, M, Pugliese, A, 2010. From thrust-and-fold belt to foreland: hydrocarbon occurrences in Italy. Geol. Soc. Lond. Petrol. Geol. Conf. Ser. 7, 113–126. doi:10.1144/0070113.

Bertotti, G, Picotti, V, Chilovi, C, Fantoni, R, Merlini, S, Mosconi, A, 2001. Neogene to quaternary sedimentary basins in the south adriatic (central Mediterranean): foredeeps and lithospheric buckling. Tectonics 771–787.

Bigi, G, Cosentino, D, Parotto, M, Sartori, R, Scandone, P, 1990. Structural model of Italy and gravity map, 1:500,000. Quad. Ric. Sci. 114 (3) S.EL.CA Florence.CROP Atlas. 2003. Memorie descrittive della Carta Geologica d'Italia, Volume LXII.

Bigi, S, Casero, P, Ciotoli, G, 2011. Seismic interpretation of the Laga basin; constraints on the structural setting and kinematics of the central Apennines. J. Geol. Soc. 168 (1), 179–190. doi:10.1144/0016-76492010-084.

Boccaletti, M, Calamita, F, Viandante, M G, 2005. La Neo-Catena litosferica appenninica nata a partire dal Pliocene inferiore come espressione della convergenza Africa-Europa. Boll. Soc. Geol. Ital. 124, 87–105.

Bulat, J, Stoker, S J, 1987. Uplift determination from interval velocity studies, UK, southern North Sea. In: Brooks, J, Glennie, K W (Eds.), Petroleum Geology of Northwest Europe. Graham & Trotman, pp. 293–305.

Casnedi, R, 1983. Hydrocarbon-bearing submarine fan system of Cellino Formation, Central Italy. AAPG (Am. Assoc. Pet. Geol.) Bull. 67, 359–370.

Cazzini, F, Dal Zotto, O, Fantoni, R, Ghielmi, M, Ronchi, P, Scotti, P, 2015. Oil and gas the Adriatic foreland, Italy. J. Petrol. Geol. 38 (3), 255–279.

Channell, J E T, D'Argenio, B, Horvath, F, 1979. Adria, the African promontory, in the Mesozoic Mediterranean palaeogeography. Earth Sci. Rev. 15, 213–292.

Dattilo, P, Pasi, R, Bertozzi, G, 1999. Depositional and structural dynamics of the Pliocene peri-adriatic foredeep, NE Italy. J. Petrol. Geol. 22, 19–36.

De Alteriis, G, 1995. Different foreland basins in Italy: examples from the central and southern Adriatic Sea. Tectonophysics 252, 349–373.

Drews, M C, Bauer, W, Caracciolo, L, Stollhofen, H, 2018. Disequilibrium compaction overpressure in shales of the Bavarian Foreland Molasse Basin: results and geographical distribution from velocity-based analyses. Mar. Petrol. Geol. 92, 37–50.

Fantoni, R, Franciosi, R, 2010. Mesozoic extension and Cenozoic compression in Po plain and adriatic foreland Suppl. 1. In: F. P. Sassi (Ed.), Nature and Geodynamics of the Lithostere in Northern Adriatic, 21. Roma: Rend. Fis. Acc. Lincei, pp. 181–196 10.1007/s12210-010-0102-4.

Faust, L Y, 1951. Seismic velocity as a function of depth and geologic time. Geophysics 16, 192–206.

Finetti, I R, 1982. Structure, stratigraphy and evolution of central Mediterranean. Bollettino di Geofisica Teorica e Applicata 24, 247–312.

Finetti, I R, 2005. CROP PROJECT: Deep Seismic Exploration of the Central Mediterranean and Italy. Elsevier B.V, Amsterdam, p. 779.

Finetti, I R, Del Ben, A, 2005. Crustal tectono-stratigraphic setting of the Adriatic Sea from new CROP seismic data. CROP Project. In: By, I R, Finetti (Eds.), Deeep Seismic Exploration of the Central Mediterranean and Italy. Elsevier, Amsterdam, pp. 519–547 Atlases in Geoscience 1.

Finetti, I R, Del Ben, A, Forlin, E, Pipan, M, Prizzon, A, Calamita, F, Crescenti, U, Rusciadelli, G, Scisciani, V, 2005. Crustal geological section across Central Italy from Corsica to the Adriatic sea based on geological and CROP seismic data. In: Finetti, I R (Ed.), CROP Project: Deep Seismic Exploration of the Central Mediterranean and Italy, Atlas in Geosciences 1. Elsevier, pp. 159–196.

Geletti, R, Del Ben, A, Busetti, M, Ramella, R, Volpi, V, 2008. Gas seeps linked tosalt structures in the Central Adriatic Sea. Basin Res. 20, 473–487.

Hubbert, K M, Rubey, W W, 1959. Role of fluid pressure in mechanics of over- trusting faulting. Bull. Am. Geogr. Soc. 70, 115–166.
Japsen, P, 1999. Overpressured Cenozoic shale mapped from velocity anomalies relative to a baseline for marine shale, North Sea. Petrol. Geosci. 5, 321–336.
Japsen, P, Mukerji, T, Mavko, G, 2007. Constraints on velocity-depth trends from rock physics models. Geophys. Prospect. 55, 135–154.
Lupa, J, Flemings, P, Tennant, S, 2002. Pressure and trap integrity in the deepwater Gulf of Mexico. Lead. Edge 21, 184–187.
Malinverno, A, Ryan, B F, 1986. Extension in the Tyrrhenian Sea and shortening in the Apennines as a result of arc migration driven sinking of the lithosphere. Tectonics 5, 227–245.
Mancinelli, P, Pauselli, C, Minelli, G, Federico, C, 2015. Magnetic and gravimetric modeling of the central Adriatic region. J. Geodyn. 89, 60–70.
Mancinelli, P, Pauselli, C, Minelli, G, Barchi, M R, Simpson, G, 2018. Potential Evidence for Slab Detachment from the Flexural Backstripping of a Foredeep: Insight on the Evolution of the Pescara Basin (Italy). Terra nova. doi:10.1111/ter.12329.
Mancinelli, P, Porreca, M, Pauselli, C, Minelli, G, Barchi, M R, Speranza, F, 2019. Gravity and magnetic modeling of central Italy: insights into the depth extent of the seismogenic layer. G-cubed 2 0. doi:10.1029/2018GC008002.
Mancinelli, P, Pauselli, C, Fournier, D, Fedi, M, Minelli, G, Barchi, M R, 2020. Three dimensional gravity local inversion across the area struck by the 2016–2017 seismic events in Central Italy. J. Geophys. Res.: Solid Earth 125, e2019JB018853. doi:10.1029/2019JB018853.
Montone, P, Mariucci, M T, 2015. P-wave velocity, density, and vertical stress magnitude along the crustal Po Plain (Northern Italy) from sonic log drilling data. Pure Appl. Geophys. 172, 1547–1561. doi:10.1007/s00024-014-1022-5.
Montone, P, Mariucci, M T, 2020. Constraints on the structure of the shallow crust in Central Italy from geophysical log data. Sci. Rep. 10, 3834. doi:10.1038/s41598-020-60855-0.
Mouchet, J-P, Mitchell, A, 1989. Abnormal Pressures while Drilling: Origins, Predictions, Detection Evaluation. Editions Technip, Paris, France.
Pace, P, Scisciani, V, Calamita, F, 2011. Styles of plio-quaternary positive inversion tectonics in the central-southern Apennines and in the adriatic foreland. Rendiconti Online della Società Geologica Italiana 15, 92–95.
Pace, P, Scisciani, V, Calamita, F, Butler, R W H, Iacopini, D, Esestime, P, Hodgson, N, 2015. Inversion structures in a foreland domain: seismic examples from the Italian Adriatic Sea. Interpretation 3, SAA161. doi:10.1190/INT-2015-0013.1.
Pauselli, C, Gola, G, Mancinelli, P, Trumpy, E, Saccone, M, Manzella, A, Ranalli, G, 2019. A new surface heat flow map of the Northern Apennines between latitudes 42.5 and 44.5 N. Geothermics 81, 39–52.
Peace, D, Brown, D, Zappaterra, E, Spoors, R, Scaife, G, Rowlands, D, Sewell, D, 2012. The Italian Adriatic Sea: bringing new life to an established region. Lead. Edge 31, 802–809. doi:10.1190/tle31070802.1.
Porreca, M, Minelli, G, Ercoli, M, Brobia, A, Mancinelli, P, Cruciani, F, Giorgetti, C, Carboni, F, Mirabella, F, Cavinato, G, Cannata, A, Pauselli, C, Barchi, M R, 2018. Seismic reflection profiles and subsurface geology of the area interested by the 2016-2017 earthquake sequence (Central Italy). Tectonics 37, 1116–1137.
Scisciani, V, 2009. Styles of positive inversion tectonics in the Central Apennines and in the Adriatic foreland: implications for the evolution of the Apennine chain (Italy). J. Struct. Geol. 31, 1276–1294.
Scisciani, V, Calamita, F, 2009. Active intraplate deformation within Adria: examples from the adriatic region. Tectonophysics 476, 57–72.
Scisciani, V, Esestime, P, 2017. The Triassic Evaporites in the Evolution of the Adriatic Basin. Permo-Triassic Salt Provinces of Europe, North Africa and the Atlantic Margins. pp. 499–516 (Chapter 23) pp. doi:10.1016/B978-0-12-809417-4.00024-0.
Scisciani, V, Montefalcone, R, 2006. Coexistence of thin- and thick-skinned tectonics: an example from the Central Apennines, Italy. Geol. Soc. Am. 33–54 Special paper 414. doi:10.1130/2006.2414(03).
Scisciani, V, Agostini, S, Calamita, F, Cilli, A, Giori, I, Pace, P, Paltrinieri, W, 2010. The influence of pre-existing extensional structures on the Neogene evolution of the Northern Apennines foreland fold-and-thrust belt. Rendiconti Online Società Geologica Italiana 10, 125–128.
Scisciani, V, Patruno, S, Tavarnelli, E, Calamita, F, Pace, P, Iacopini, D, 2019. Multi-phase Reactivations and Inversions of Paleozoic-Mesozoic Extensional Basins during the Wilson Cycle: Case Studies from the North Sea (UK) and Northern Apennines (Italy). Geological Society, London, Special Publications. doi:10.1144/SP470-2017-232.
Scrocca, D, 2006. Thrust front segmentation induced by differential slab retreat in the Apennines (Italy). Terra. Nova 18, 154–161.
Scrocca, D, Carminati, E, Doglioni, C, Marcantoni, D, 2005. Slab retreat and active shortening along the central-northern Apennines. Thrust belts and foreland basins: from fold kinematics to hydrocarbon systems book series. Front. Earth Sci. 471–487.
Sibson, R, 1981. Controls on low-stress hydro-fracture dilatancy in thrust, wrench and normal fault terrains. Nature 289, 665–667.
Simpson, G, 2014. Decoupling of foreland basin subsidence from topography linked to faulting and erosion. Geology 42 (9), 775–778.
Slotnik, M M, 1936. On seismic computations, with applications, II. Geophysics 1, 299–305.
Stampfli, G M, Borel, G D, Marchant, R, Mosar, J, 2002. Western Alps geological constraints on western Tethian reconstructions. In: Rosenbaum, G, Lister, G S (Eds.), Reconstruction of the Evolution of the Alpine-Himalayan Orogen. Journal of the Virtual Explorer, 8. pp. 77–106.
Tarquini, S, Isola, I, Favalli, M, Boschi, E, 2007. TINITALY/01: a new triangular irregular network of Italy. Ann. Geophys. 50–53.
Tarquini, S, Vinci, S, Favalli, M, Doumaz, F, Fornaciai, A, Nannipieri, L, 2012. Release of a 10-m-resolution DEM for the Italian territory: comparison with global-coverage DEMs and anaglyph-mode exploration via the web. Comput. Geosci. 38, 168–170.
Tavarnelli, E, Scisciani, V, Patruno, S, Calamita, F, Pace, P, Iacopini, D, 2019. The role of structural inheritance in the evolution of fold-and-thrust belts: insights from the Umbria-Marche Apennines, Italy. Geol. Soc. Am. Spec. Pap. 542, 191–211. doi:10.1130/2019.2542(10.
Tobin, H J, Saffer, D M, 2009. Elevated fluid pressure and extreme mechanical weakness of a plate boundary thrust, Nankai Trough subduction zone. Geology 37, 679–682.
Vai, G B, 2001. Basement and early (pre-Alpine) history. In: Vai, G B, Martini, I P (Eds.), Anatomy of an Orogen: the Apennines and Adjacent Mediterranean Basins. Kluwer Academic Publishers, Dordrecht/Boston/London, pp. 121–150.
Venisti, N, Calcagnile, G, Pontevivo, A, Panza, G F, 2005. Tomographic study of the adriatic plate. Pure Appl. Geophys. 162, 311–329.